Supporting Information

Disentangling an extended network of Rh complexes in Supported Ionic Liquid Phase (SILP) catalysts for hydroformylation: A combined *in situ* IRAS and DFT study

Kailun Zhang[1], Sophie Mayer[2], Sharmin Khan Antara[3], Arsha M. Cherian[4], Huiyi Xu[1], Ana-Sunčana Smith[4,5], Nicolas Vogel[2], Marco Haumann[3,6], Christian R. Wick[4*], Tanja Retzer[1*]

[1]Interface Research and Catalysis, ECRC, Friedrich-Alexander-Universität Erlangen-Nürnberg, Egerlandstraße 3, 91058 Erlangen, Germany

[2]Institute of Interfaces and Particle Technology, Friedrich-Alexander-Universität Erlangen-Nürnberg, Cauerstraße 4, 91058 Erlangen, Germany

[3]Lehrstuhl für Chemische Reaktionstechnik, Friedrich-Alexander-Universität Erlangen-Nürnberg, Egerlandstraße 3, 91058 Erlangen, Germany

[4]PULS Group and Computational Advanced Materials and Processes (CAMP), Friedrich-Alexander-Universität Erlangen-Nürnberg, IZNF, Erlangen 91058, Germany

[5] Group for Computational Life Sciences, Division of Physical Chemistry, Ruđer Bošković Institute, Zagreb 10000, Croatia

[6] Research Centre for Synthesis and Catalysis, Department of Chemistry, University of Johannesburg, P.O. Box 524, Auckland Park 2006, South Africa

*corresponding authors: Tanja Retzer, tanja.retzer@fau.de; Christian R. Wick: christian.wick@fau.de

1. Preparation of SILP catalyst

Table S1. Reagent-specific information on SILP catalysts for catalytic testing in berty reactors

Material	CAS number	Supplier	Purity
Acetylacetonato(dicarbonyl)rhodium(I)	14874-82-9	Sigma-Aldrich	98%
Xantphos	161265-03-8	Sigma-Aldrich	97%
1-Butyl-3-methylimidazolium-bis(trifluormethylsulfonyl)amide	174899-83-3	Iolitec	99%
Silica 150	112926-00-8	Carl Roth	99.3%
Dichlormethane	75-09-2	Sigma-Aldrich	99.8%
Helium	7440-59-7	Air Liquide	99.999%
Ethene	74-85-1	Linde	99.9%
Hydrogen	1333-74-0	Air Liquide	99.999%
Carbonmonoxide	630-08-0	Air Liquide	99.97%

2. Sample Preparation for TIRS

Table S2.

Solutions	Rh-precursor / mg	Xantphos / mg	IL / mg
1	1.7	0.0	0.0
2	0.0	16.8	0.0
3	0.0	0.0	25
4	1.7	0.0	10
5	1.7	0.0	25
6	0.0	16.8	25
7	1.7	16.8	0.0
8	1.7	16.8	25

Each solution was obtained by dissolving the substances in the above table into 1 mL of DCM.

3. Experimental procedure for *in situ* IRAS

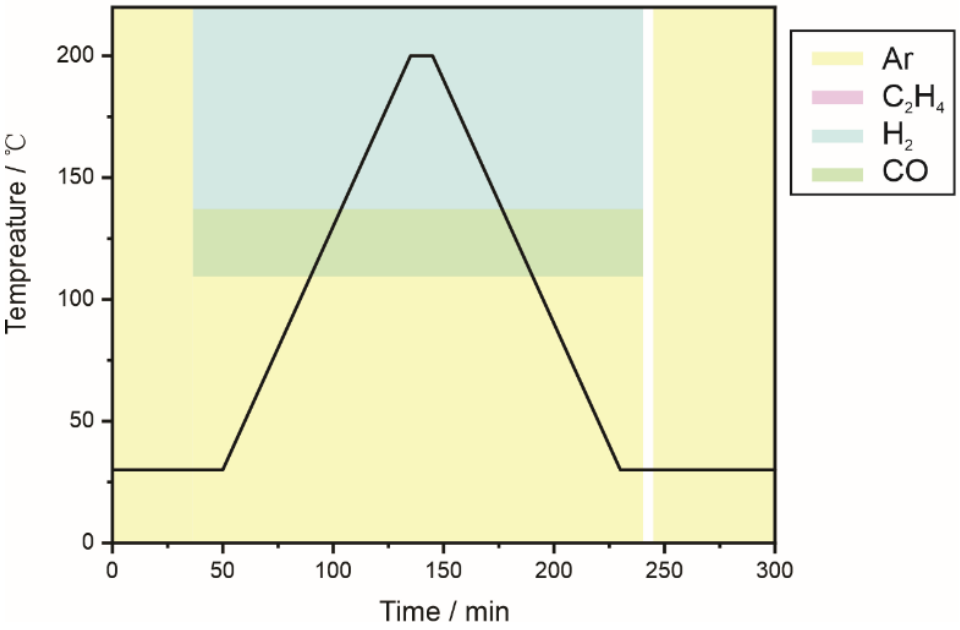

Figure S1: heating ramp and applied gas atmosphere of IRAS measurements. Reaction conditions: T = 30–200 °C, p = 1 bar, 2.6 ml_N min^{-1} H_2, 0.9 ml_N min^1 CO, 2.5 ml_N min^1 Ar.

Table S3. Preparation of the solution for IRAS experiments

Solutions	Rh-precursor / mg	Xantphos / mg	IL / mg
1	1.9	0.0	0.0
2	0.0	16.8	0.0
3	0.0	0.0	100
4	1.9	16.8	0.0
5	1.9	0.0	100
6	0.0	16.8	100

Each solution was obtained by dissolving the substances in the above table into 1 mL of DCM.

4. Comparison of experimental and DFT-computed spectra

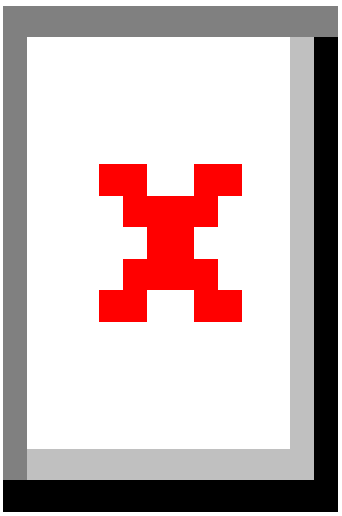

Figure S2: Comparison of experimental (downwards-pointing) and DFT-computed (upwards-pointing, scaling factor 1.012) IR spectra for xantphos and [Rh(acac)$(CO)_2$]. The spectral region at ~1300 cm-1 suffers from total absorption due to the DCM solvent and is therefore greyed out.

5. Formation of catalyst precursors: T1 and FOD multireference diagnostics

Table S4: T1 and Fractional Occupation Number Weighted Density (FOD) multireference diagnostics for the species involved in the formation of the catalyst precursors.

Species	N_FOD	T1
$[Rh(acac)(CO)_2]$+xp (**1**)	0.55	0.015
$[Rh(acac)(CO)_2(xp)]$ (**2a**)	0.58	0.015
[Rh(acac)(CO)(xp)] (**3b**) + CO	0.60	0.015
[Rh(acac)(CO)(xp)] (**3a**) + CO	0.88	0.015
$TS_{(1)-(2)}$	0.62	0.015
$TS_{(2)-(3)}$	0.58	0.015

6. Reproducibility of Hydroformylation of ethene in the Berty reactor using SILP catalyst and calculation of TOF values

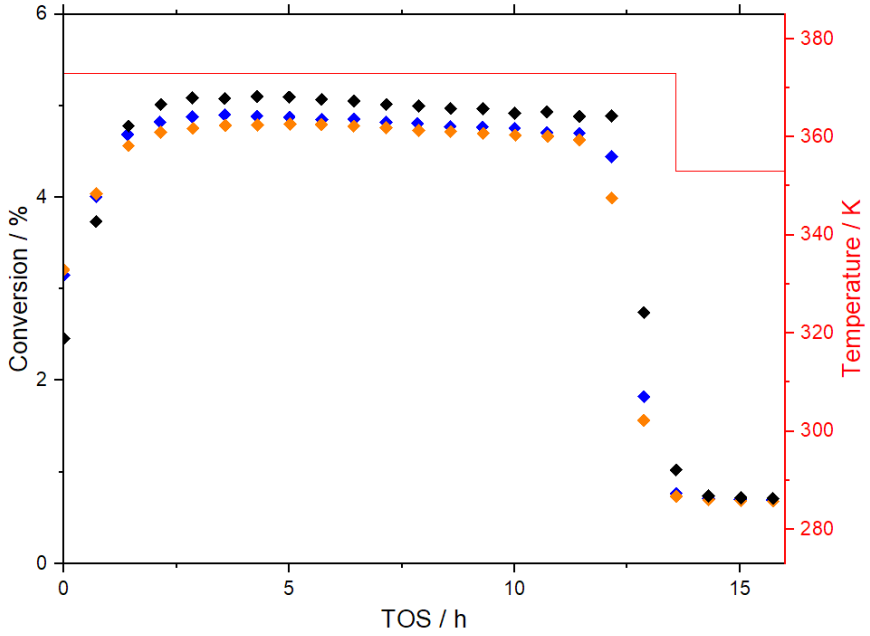

Figure S3: Reproducibility of Hydroformylation of ethylene in the Berty reactor using SILP catalyst consisting of $Rh(acac)(CO)_2$:xantphos in 1:4 ratio dissolved in $[C_2C_1Im][NTf_2]$ and supported on silica 150, particle size 350-500 µm, IL loading is α_{IL} = 30%. Ethylene conversion at 353, and 373 K for the same catalyst prepared three times. Reaction conditions: 1.0 g catalyst, 0.2 wt.% Rh, Temp: 353 – 373 K, 1.1 MPa, 15 ml_N min^{-1} C_2H_4, 30 ml_N min^{-1} H_2, 30 mlN min^{-1} CO, average residence time 185 s.

The conversion X and turnover frequency (TOF) were calculated as follows based on the peak areas obtained from the GC signals and the flowrates.

$$X = 1 - \frac{c_{Ethene}}{c_{Ethene,0}} = 1 - \frac{\frac{A_{Ethene}}{2}}{\frac{A_{Ethene}}{2} + \frac{A_{Ethane}}{2} + \frac{A_{Propanal}}{3} + \frac{A_{C_6}}{6}}$$

$$\dot{n}_{Ethene,0} = \frac{p\,\dot{V}}{R\,T} = \frac{1\ bar\ 15\frac{ml_n}{min}}{8.314\frac{J}{mol\,K}\ 292{,}15\ K}\ 60\frac{min}{h} = 0.03705\frac{mol}{h}$$

$$TOF = \frac{X\,\dot{n}_{Ethene,0}}{n_{cat}}$$

7. Extension of Table 1 with different isomers of 7a-b and 9a-d

Table S5. Peak assignment via DFT, all wavenumbers in cm^{-1}.

Nr.	Species	ν_{exp}		ν_{DFT}		$\nu_{DFT} - \nu_{exp}$
7a	$[Rh(NTf_2)_2(CO)_2]^-$	2022		2025 *(vs)*		_3
	(cis, κN)	2071	_Δ = 49	2097 *(s)*	_Δ = 72	_26
7c	$[Rh(NTf_2)_2(CO)_2]^-$	2022		2019 *(vs)*		_(-3)
	(trans, κN)	2071	_Δ = 49	2089 *(vs)*	_Δ = 70	_18
9b	$[HRh(NTf_2)(CO)(xp)]^-$	<1975		1926 *(vs)*		>(−49)
	(ea, κN)	2016	_Δ > 41	2028 *(w)*	_Δ = 102	12
9c	$[HRh(NTf_2)(CO)(xp)]^-$	<1975		1931 *(vs)*		>(−44)
	(ea, κO)	2016	_Δ > 41	2015 *(w)*	_Δ = 84	_(−1)
9d	$[HRh(NTf_2)(CO)(xp)]^-$	<1975		1951 *(m)*		>(−24)
	(ee, κN)	2075	_Δ > 100	2081 *(w)*	_Δ = 131	_6
10a	*distal*-	1975		1976 *(vs)*		_1
	$[Rh(xp)(nhc)(CO)_2]^+$ *(ea)*	2016	Δ = 41	2018 *(vw)*	Δ = 42	_2
10b	*distal*-	1975		1990 *(vs)*		_15
	$[Rh(xp)(nhc)(CO)_2]^+$ *(ee)*	2016	Δ = 41	2051 *(vs)*	Δ = 61	_35

8. Difference spectra

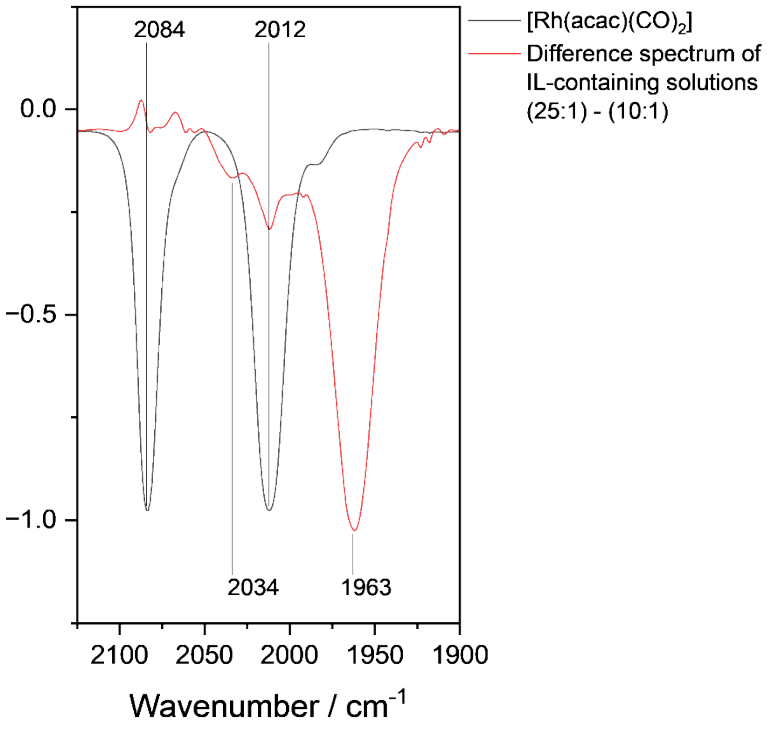

Figure S4: Difference spectra of the TIRS spectra

9. Assignment of bands of the acac ligand

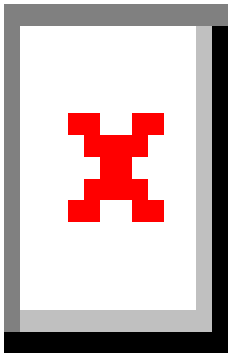

Figure S5: Comparison of acac bands of the Rh precursor [Rh(acac)$(CO)_2$] (**1**) and [Rh(acac)$(CO)_2$(xp)] *(trig. bipy.)* (**2a**) and [Rh(acac)(CO)(xp)] (**3**) (see **Table S6**), spectrum of xantphos added for sake of comparison.

Table S6. Peak assignment via DFT, all wavenumbers in cm^{-1}.

Nr.	Species	ν_{exp}		ν_{DFT}		$\nu_{DFT} - \nu_{exp}$
1	[Rh(acac)$(CO)_2$]	1526		1537 *(m)*		_11
		1568	_Δ = 42	1562 *(m)*	_Δ = 25	_(-6)
2a	[Rh(acac)$(CO)_2$(xp)] *(trig. bipy.)*	1485		1474 *(vw)*		_(-11)
		1517	_Δ = 31	1516 *(m)*	_Δ = 42	_(-1)
		1580	_Δ = 63	1601 *(m)*	_Δ = 85	_21
3	[Rh(acac)(CO)(xp)] *(sq. pyr.)*	1485		1480 *(vw)*		_(-5)
		1517	_Δ = 31	1516 *(w)*	_Δ = 36	_(-1)
		1580	_Δ = 63	1576 *(m)*	_Δ = 60	_(-4)

10. Formation of $[Rh(acac)(NTf_2)(CO)]^-$

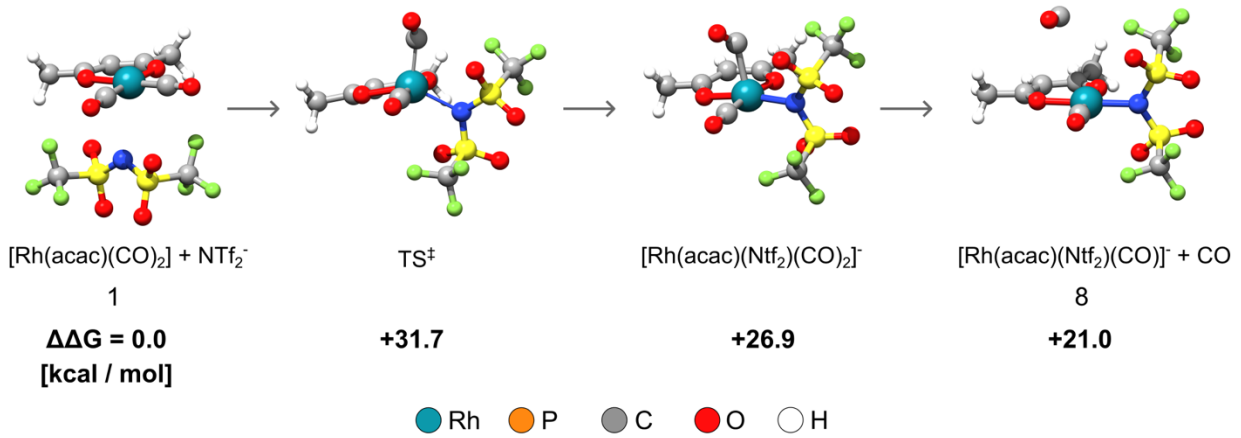

Figure S6: Formation of $[Rh(acac)(NTf_2)(CO)]^-$ computed at the SMD-ωB97M-V/ma-def2-TZVPP // SMD-BP86-D3/ma-def2-TZVP level of theory.

11. Contact angle measurements

Table S7: Contact Angle data from sessile drop measurements on different substrates using water (indicating the hydrophobicity) and $[C_4C_1Im][NTf_2]$ (IL used in catalytic test reactions).

Sample	Contact Angle [°]	
	H_2O	$[C_4C_1Im][NTf_2]$
SiO_2/Au	80.8 ± 0.9 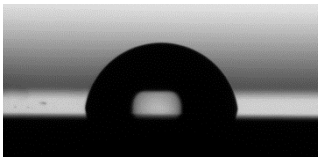	31.7 ± 0.5 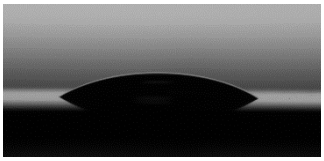
SiO_2/Au using LudoxTM beads (22 nm)	18.1 ± 4.2 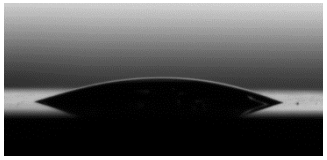	10.2 ± 0.6 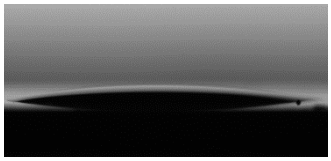
SiO_2/Au using LudoxHS beads (12 nm)	19.5 ± 2.4 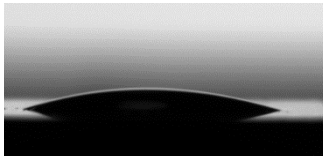	10.9 ± 0.7 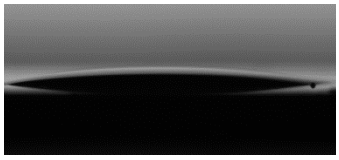

Contact angle data of the different substrates using sessile drop measurements: As test liquid water and $[C_4C_1Im][NTf_2]$ were used (2 µL droplets each). Water was used to indicate the hydrophilicity of the substrate. The IL was to mimic the catalytic test reaction conditions. The droplets were allowed to equilibrate for 60 s. The contact angle was analyzed with the help of the Tangent-1 fitting model using the Drop Shape Analyzer (DSA 25E, Krüss). In case of contact angle below 15°, the fitting method "Höhe-Breite" was used for the analysis.

12. In situ IRAS of $[C_4C_1Im][NTf_2]$ SILP wafer in H_2/CO

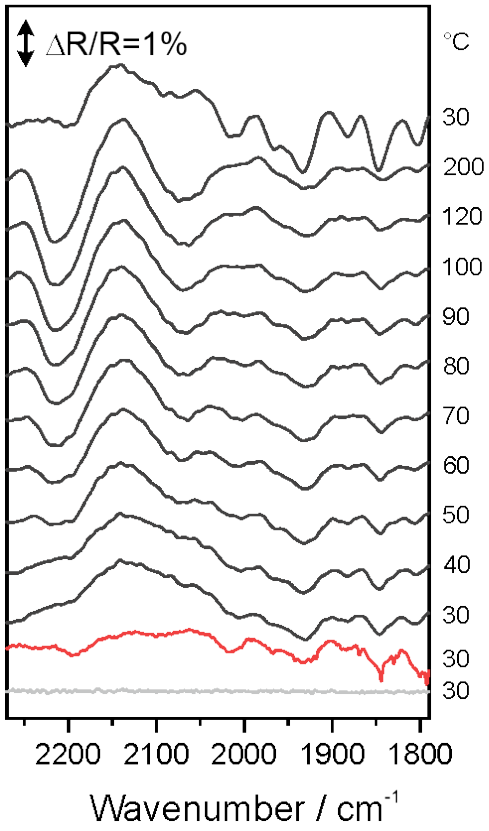

Figure S7: In-situ IR spectra of model SILP system under different atmospheres and temperatures: system with : a) $[C_4C_1Im][NTf_2]$ exposed to CO/H_2; b) $[Rh(acac)(CO)_2]$+ $[C_4C_1Im][NTf_2]$ exposed to CO/H_2; t post-analysis included subtraction of the CO gas phase according to[27].

13. Reference spectra of $[C_4C_1Im][NTf_2]$ in ATR and TIRS

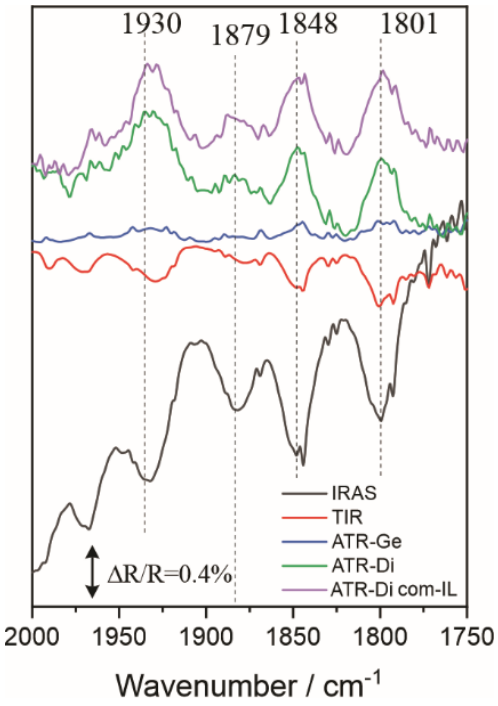

Figure S8: $[C_4C_1Im][NTf_2]$ recorded in ATR and TIRS mode. Commercial IL shorten in com-IL, Ge and Di refer to germanium and diamond applied as ATR crystals.

14. Full List of computed IR species

Table S8: List of computed IR spectra. All wavenumbers in cm^{-1}, energies in kcal mol^{-1}. Species S1-13 are not assigned to bands in the experimental spectra due to poor agreement and included at the bottom for sake of completeness. For visualization of all species see **Figures S7-S19**. Enthalpies (20 °C) are computed relative to species 1, assuming the reactions delineated in the manuscript in Figure **4** and Figure **6**.

Nr.	Species	ν_{DFT}		ΔH_{gas}	ΔH_{solv}
1	[Rh(acac)$(CO)_2$]	2021 *(vs)* 2085 *(vs)*	 Δ = 64	0.0	0.0
2a	[Rh(acac)$(CO)_2$(xp)] *(trig. bipy.)*	1984 *(vs)* 2040 *(vs)*	 Δ = 56	-23,7	-20,6
2b	[Rh(acac)$(CO)_2$(xp)] *(sq. pyr.)*	1929 *(vs)* 2000 *(s)*	 Δ = 71	-15,7	-16,6
3a	[Rh(acac)(CO)(xp)] *(sq. pyr.)*	1968 *(vs)*		-16,4	-11,6
3b	[Rh(acac)(CO)(xp)] *(sq. pl.)*	1988 *(vs)*		-11,3	-7,7
3c	[Rh(acac)(CO)(xp)] *(trig. bipy.)*	1978 *(vs)*		-6,2	-2,8
4a	*distal*-[HRh$(CO)_2$(xp)] *(ea)*	1960 *(vs)* 1998 *(m)* 2018 *(w)*	 Δ = 37 Δ = 20	-39,5	-41,4
4b	*distal*-[HRh$(CO)_2$(xp)] *(ee)*	1949 *(w)* 1989 *(vs)* 2059 *(m)*	 Δ = 40 Δ = 70	-39,7	-40,4
4c	*prox*-[HRh$(CO)_2$(xp)] *(ea)*	1963 *(vs)* 2002 *(m)*	 Δ = 39	-30,0	-32,3
4d	*prox*-[HRh$(CO)_2$(xp)] *(ee)*	1964 *(m)* 1997 *(vs)* 2076 *(s)*	 Δ = 33 Δ = 80	-26,4	-27,6
5a	*distal*-[HRh(CO)(xp)] *(cis)*	1986 *(vs)*		-5,1	-4,3
5b	*prox*-[HRh(CO)(xp)] *(cis)*	1983 *(vs)*		-1,5	-1,1
5c	*distal*-[HRh(CO)(xp)] *(trans)*	1929 *(w)* 2032 *(vs)*	 Δ = 103	0,3	1,1
5d	*prox*-[HRh(CO)(xp)] *(trans)*	1993 *(vs)*		0,9	1,9
6a	[Rh(NTf_2)(CO)(xp)]$^-$ *(VdW., sq. pl.)*	2024 *(vs)*		22,9	5,1

Nr.	Species	ν_{DFT}		ΔH_{gas}	ΔH_{solv}
6b	$[Rh(NTf_2)(CO)(xp)]^-$ *(kN, sq. pyr.)*	2005 *(vs)*		26,3	7,8
6c	*distal*-$[Rh(NTf_2)(CO)(xp)]^-$ *(trans, kO)*	2000 *(vs)*		24,8	10,9
6d	*distal*-$[Rh(NTf_2)(CO)(xp)]^-$ *(trans, kN)*	1999 *(vs)*		27,0	11,4
6e	*distal*-$[Rh(NTf_2)(CO)(xp)]^-$ *(cis, kN)*	2022 *(vs)*		28,1	11,5
6f	*distal*-$[Rh(NTf_2)(CO)(xp)]^-$ *(cis, kO)*	2039 *(vs)*		30,5	15,8
7a	$[Rh(NTf_2)_2(CO)_2]^-$*(cis, kN)*	2018 *(vs)* 2089 *(vs)*	 Δ = 71	28,7	19,8
7b	$[Rh(NTf_2)_2(CO)_2]^-$*(cis, kN-O)*	2025 *(vs)* 2097 *(s)*	 Δ = 72	30,3	23,8
7c	$[Rh(NTf_2)_2(CO)_2]^-$ *(trans, kN)*	2019 *(vs)*		35,9	30,3
7d	$[Rh(NTf_2)_2(CO)_2]^-$ *(cis, kO-O)*	2030 *(m)* 2101 *(m)*	 Δ = 72	37,7	32,7
8a	$[Rh(acac)(NTf_2)(CO)]^-$*(kN)*	1978 *(vs)*		20,3	25,9
8b	$[Rh(acac)(NTf_2)(CO)]^-$*(kO)*	1989 *(vs)*		29,3	35,5
9a	$[HRh(NTf_2)(CO)(xp)]^-$*(VdW, ea)*	1956 *(vs)* 2024 *(vw)*	 Δ = 68	-22,0	-14,0
9b	*distal*-$[HRh(NTf_2)(CO)(xp)]^-$*(ea, kN)*	1926 *(vs)* *2028* (w)	 Δ = 103	-22,8	-14,0
9c	*distal*-$[HRh(NTf_2)(CO)(xp)]^-$*(ea, kO)*	1931 *(vs)* 2015 *(w)*	 Δ = 83	-22,2	-12,3
9d	*distal*-$[HRh(NTf_2)(CO)(xp)]^-$*(ee, kN)*	1951 *(m)* *2081* (w)	 Δ = 131	-20,9	-12,0
9e	*distal*-$[HRh(NTf_2)(CO)(xp)]^-$*(ee, kO)*	1936 *(w)* *2063(w)*	 Δ = 127	-17,0	-7,6
9f	$[HRh(NTf_2)(CO)(xp)]^-$*(VdW, ee)*	2007 *(vs)*		-12,6	-6,7
10a	*distal*-$[Rh(CO)_2(nhc)(xp)]^+$ (*ea*)	1976 (vs) 2018 (w)	 Δ = 42	-48.3	-46.9
10b	*distal*-$[Rh(CO)_2(nhc)(xp)]^+$ (*ee*)	1990 (vs) 2051 (vs)	 Δ = 61	-45.4	-43.9

Nr.	Species	ν_{DFT}		ΔH_{gas}	ΔH_{solv}
S1	$[Rh(NTf_2)(CO)_2]$	2048 *(vs)* 2114 *(s)*	 $\Delta = 66$	61,2	45,0
S2a	$[Rh(NTf_2)(CO)_3]$ (*kN)*	2075 *(s)* 2101 *(vs)* 2176 *(vw)*	 $\Delta = 26$ $\Delta = 75$	37,9	14,8
S2b	$[Rh(NTf_2)(CO)_3]$ (*kO)*	2079 *(s)* 2108 *(vs)* 2182 *(vw)*	 $\Delta = 29$ $\Delta = 74$	48,2	26,2
S2c	$[Rh(NTf_2)(CO)_3]$ (*kO-O)*	2079 *(vs)* 2152 *(vw)*	 $\Delta = 73$	49,0	28,2
S3a	*distal*-$[Rh(CO)_2(xp)]^+$ *(trans)*	2039 *(s)* 2092 *(vs)*	 $\Delta = 53$	75,3	-4,1
S3b	*proximal*-$[Rh(CO)_2(xp)]^+$ *(trans)*	2011 *(vs)* 2057 *(w)*	 $\Delta = 46$	75,8	-2,9
S3c	*distal*-$[Rh(CO)_2(xp)]^+$ *(cis)*	2002 *(vs)* 2052 *(w)*	 $\Delta = 50$	77,8	-2,0
S3d	*proximal*-$[Rh(CO)_2(xp)]^+$ *(cis)*	2042 *(s)* 2093 *(vs)*	 $\Delta = 51$	78,8	-0,7
S4a	$[Rh(CO)_2(xp)]$ *(cis)*	1937 *(s)* 1973 *(vs)*	 $\Delta = 36$	-	-
S4b	$[Rh(CO)_2(xp)]$ *(trans)*	1922 *(vs)* 1967 *(w)*	 $\Delta = 44$	-	-
S5	$[HRh(NTf_2)(CO)_2]^-$	1981 *(vs)* 2045 *(m)*	 $\Delta = 64$	0,9	5,0
S6	$[HRh(NTf_2)_2(CO)]^{2-}$	1958 *(s)*		93,9	50,8
S7	$[HRh(CO)_4]$	2011 *(vw)* 2042 *(vs)* 2079 *(vw)* 2128 *(vw)*	 $\Delta = 32$ $\Delta = 37$ $\Delta = 50$	-28,6	-32,6
S8	$[HRh(CO)_3]$	2045 *(vs)* 2066 *(m)*	 $\Delta = 21$	-5,6	-8,9

Nr.	Species	ν_{DFT}		ΔH_{gas}	ΔH_{solv}
S9	$[HRh(NTf_2)(CO)_3]^-$	1959 *(vw)* 1987 *(vs)* 2024 *(w)* 2084 *(w)*	 Δ = 29 Δ = 37 Δ = 60	-23,6	-21,1
S10	$[Rh(CO)_4]^+$	2147 *(vs)*		133,7	22,0
S11	$[Rh_2(CO)_8]$	1886 *(w)* 2053 *(vs)* 2076 *(m)*	 Δ = 167 Δ = 23	-	-
S12	$[Rh_2(CO)_6]$	1909 *(m)* 2039 *(s)* 2061 *(vs)*	 Δ = 130 Δ = 22	-	-
S13	$[Rh_4(CO)_{12}]$	1907 *(w)* 2042 *(w)* 2072 *(vs)*	 Δ = 136 Δ = 30	-	-
S14	[Rh(acac)(CO)(nhc)]	1986 (vs)		-17,3	-10,9
S15a	$[HRh(CO)_2(nhc)]$ *(sq. pl.)*	2006 (vs) 2053 (s)	 Δ = 46.9	-	-
S15b	$[HRh(CO)_2(nhc)]$ *(dist. sq. pl.)*	1968 (vs) 2031 (w)	 Δ = 63.6	-	-
S16	$[H_2Rh(acac)(CO)(nhc)]$	2043 (vs) 2159 (w)	 Δ = 115.7	-	-
S17a	$[Rh(CO)_2(nhc)_2]^+$ (*cis*)	2045 (vs) 2092 (vs)	 Δ = 46.9	-	-
S17b	$[Rh(CO)_2(nhc)_2]^+$ (*trans*)	2017 (vs) 2086 (vw)	 Δ = 68.9	-	-
S18a	$[HRh(CO)(nhc)_2]$ (*cis*)	1860 (w) 1968 (vs)	 Δ = 107.2	-	-
S18b	$[HRh(CO)(nhc)_2]$ (trans)	1956 (vs)			
S19a	*distal*-$[Rh(CO)(nhc)(xp)]^+$ *(cis)*	2000 (vs)		-23.6	-24.1
S19b	*distal*-$[Rh(CO)(nhc)(xp)]^+$ *(trans)*	2009 (vs)		-22.4	-22.7
S19c	*proximal*-$[Rh(CO)(nhc)(xp)]^+$ (*cis*)	2010 (vs)		-19.7	-20.1
S19d	*proximal*-$[Rh(CO)(nhc)(xp)]^+$ (*trans*)	2030 (vs)		-18.3	-18.7

Nr.	Species	ν_{DFT}		ΔH_{gas}	ΔH_{solv}
S20a	*distal*-[HRh(CO)(CO)(xp)] (*ee*)	1927 (vs) 1977 (vw)	$\Delta = 50.1$	-	-
S20b	*distal*-[HRh(CO)(nhc)(xp)] (*ea*)	1934 (vs) 1981 (w)	$\Delta = 46.7$	-	-

15. Visualisation of all DFT-optimized complexes

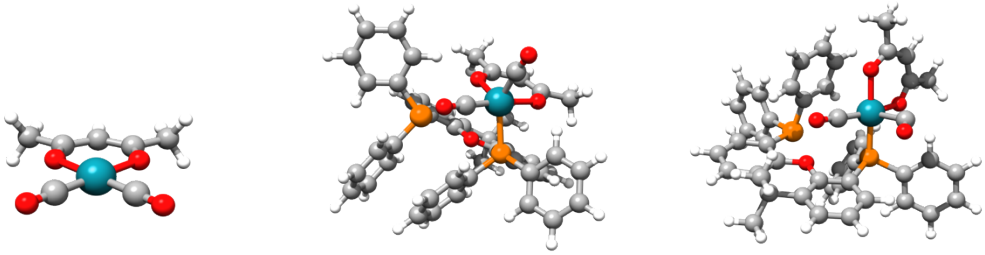

[Rh(acac)(CO)$_2$]
(**1**)

[Rh(acac)(CO)$_2$(xp)]
(**2a**)
ΔG = -20.6

[Rh(acac)(CO)$_2$(xp)]
(**2b**)
ΔG = -16.6

Figure S9: Visualisation of all isomers of DFT-optimized species **1** and **2**. Note that xantphos binds in monodentate fashion in species **2**.

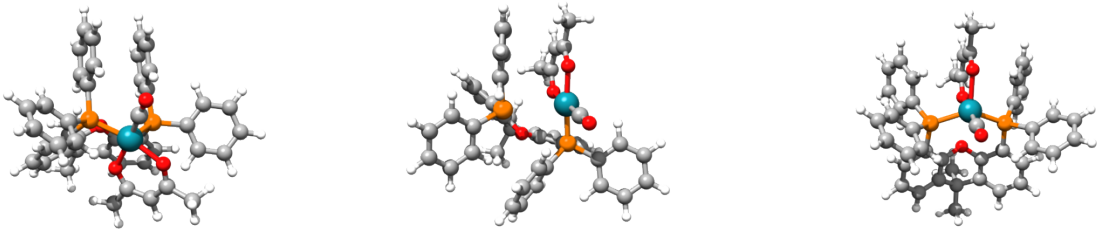

[Rh(acac)(CO)(xp)]
(**3a**)
ΔG = -11.6

[Rh(acac)(CO)(xp)]
(**3b**)
ΔG = -7.7

[Rh(acac)(CO)(xp)]
(**3c**)
ΔG = -2.8

Figure S10: visualisation of all isomers of DFT-optimized species **3**. Note that xantphos binds in monodentate fashion in species **3b**.

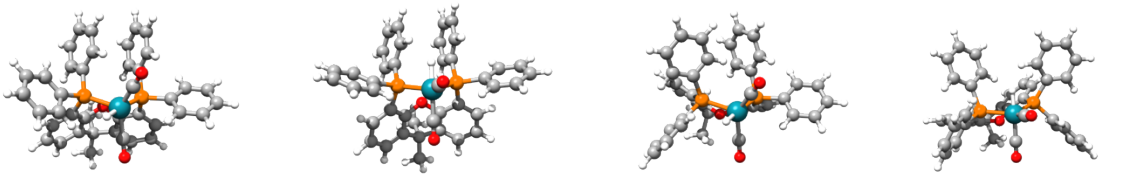

distal-[HRh(CO)$_2$(xp)] *(ea)*
(**4a**)
ΔG = -41.4

distal-[HRh(CO)$_2$(xp)] *(ee)*
(**4b**)
ΔG = -40.4

prox-[HRh(CO)$_2$(xp)] *(ea)*
(**4c**)
ΔG = -32.2

prox-[HRh(CO)$_2$(xp)] *(ee)*
(**4d**)
ΔG = -27.6

Figure S11: visualisation of all isomers of DFT-optimized species **4**.

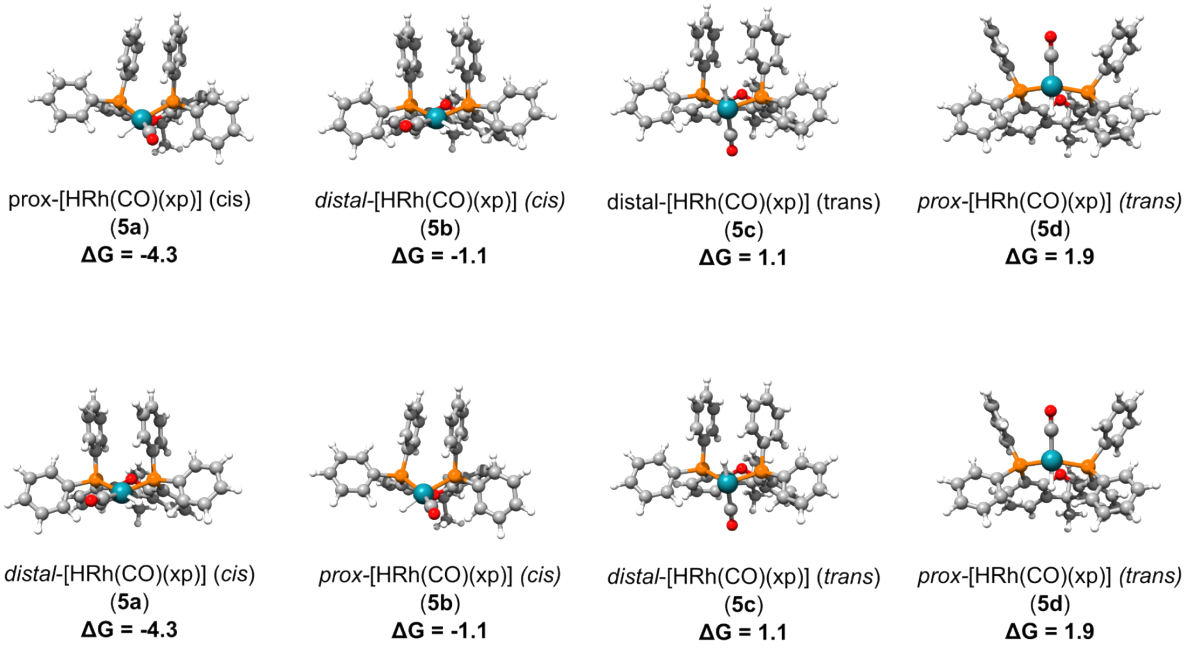

Figure S12: visualisation of all isomers of DFT-optimized species **5**.

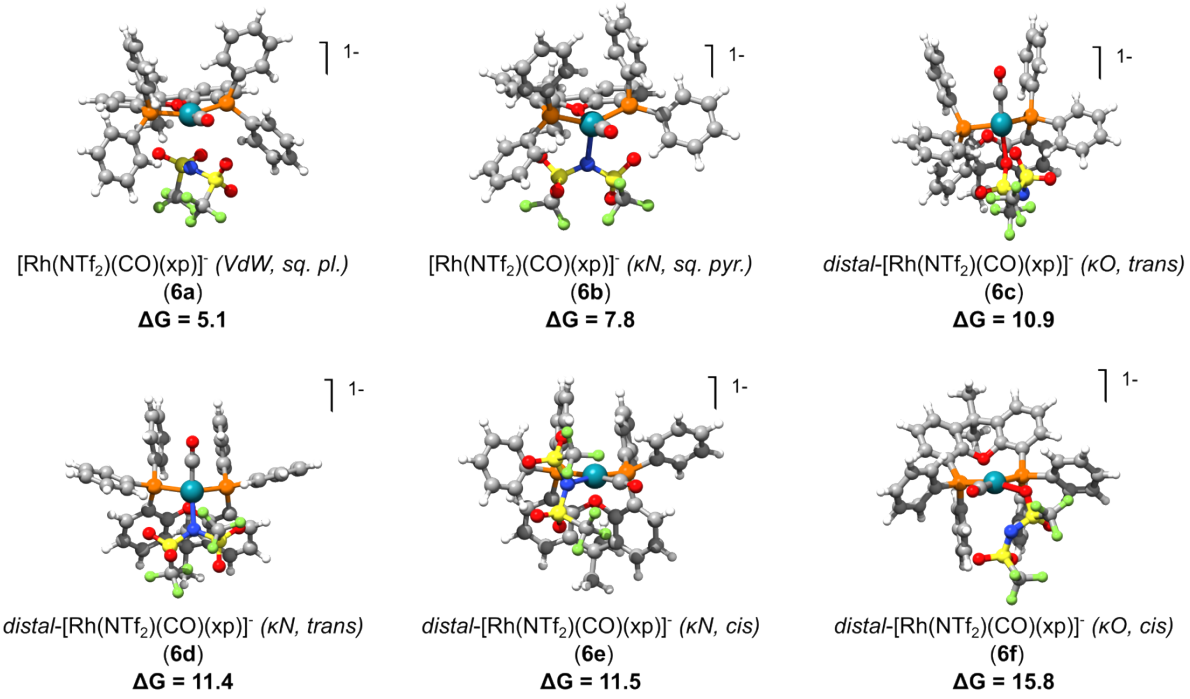

Figure S13: visualisation of all isomers of DFT-optimized species **6**. Note that xantphos binds in tridentate fashion in species **6a** and **6b** as indicated by Mayer bond orders of 0.36 for the Rh-O bonds.

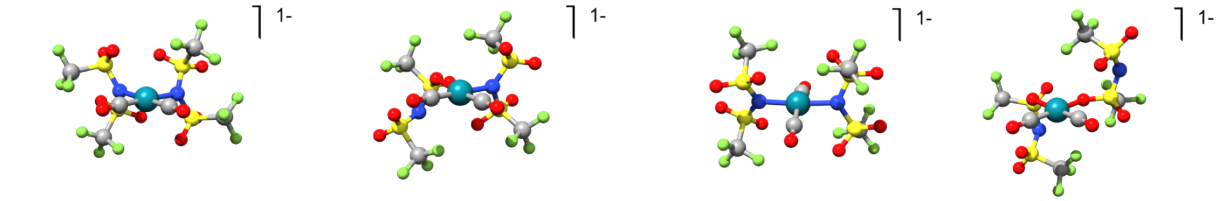

[Rh(NTf$_2$)$_2$(CO)$_2$]$^-$ *(κN-N,cis)* (**7a**) **ΔG = 19.8**

[Rh(NTf$_2$)$_2$(CO)$_2$]$^-$ *(κN-O, cis)* (**7b**) **ΔG = 23.8**

[Rh(NTf$_2$)$_2$(CO)$_2$]$^-$ *(κN-N, trans)* (**7c**) **ΔG = 30.3**

distal-[Rh(NTf$_2$)$_2$(CO)$_2$]$^-$ *(κO-O, cis)* (**7d**) **ΔG = 32.7**

Figure S14: visualisation of all isomers of DFT-optimized species **7**.

[Rh(acac)(NTf$_2$)(CO)]$^-$ *(κN)* (**8a**) **ΔG = 25.9**

[Rh(acac)(NTf$_2$)(CO)]$^-$ *(κO)* (**8b**) **ΔG = 35.5**

Figure S15: visualisation of all isomers of DFT-optimized species **8**.

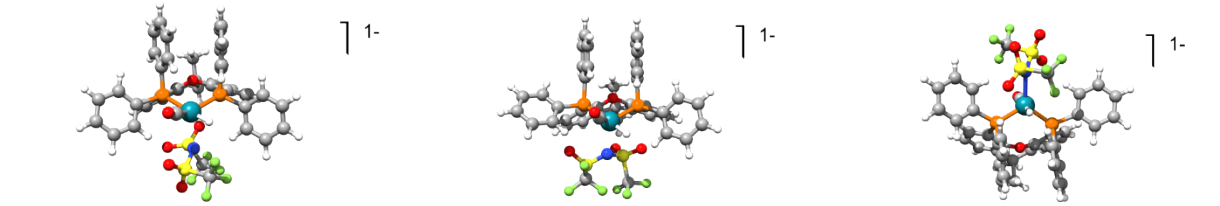

distal-[HRh(NTf$_2$)(CO)(xp)]$^-$ *(VdW, ea)* (**9a**) **ΔG = -14.0**

distal-[HRh(NTf$_2$)(CO)(xp)]$^-$ *(κN, ea)* (**9b**) **ΔG = -14.0**

distal-[HRh(NTf$_2$)(CO)(xp)]$^-$ *(κO, ea)* (**9c**) **ΔG = -12.3**

distal-[HRh(NTf$_2$)(CO)(xp)]$^-$ *(κN, ee)* (**9d**) **ΔG = -12.0**

distal-[HRh(NTf$_2$)(CO)(xp)]$^-$ *(κO,ee)* (**9e**) **ΔG = -7.6**

distal-[HRh(NTf$_2$)(CO)(xp)]$^-$ *(VdW, ee)* (**9f**) **ΔG = -6.7**

Figure S16: visualisation of all isomers of DFT-optimized species **9**.

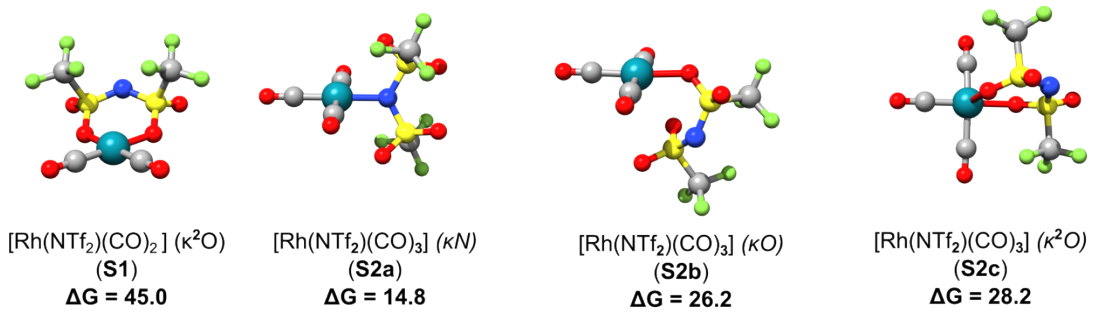

Figure S17: visualisation of all isomers of DFT-optimized species **S1** and **S2**.

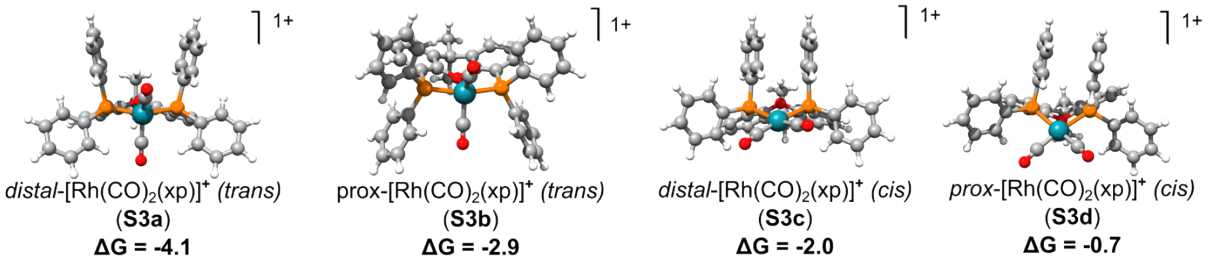

Figure S18: visualisation of all isomers of DFT-optimized species **S3.**

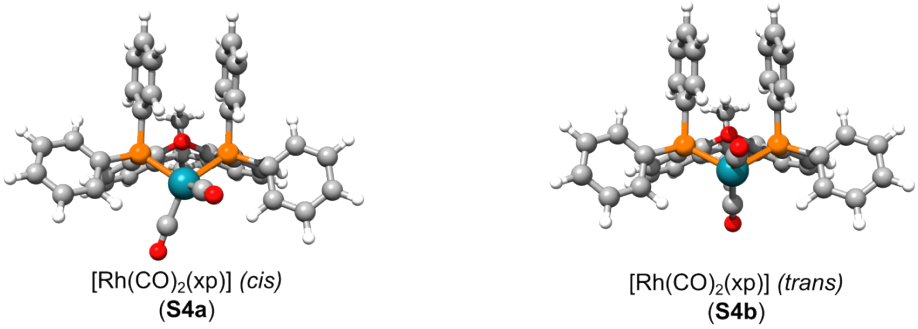

Figure S19: visualisation of all isomers of DFT-optimized species **S4.**

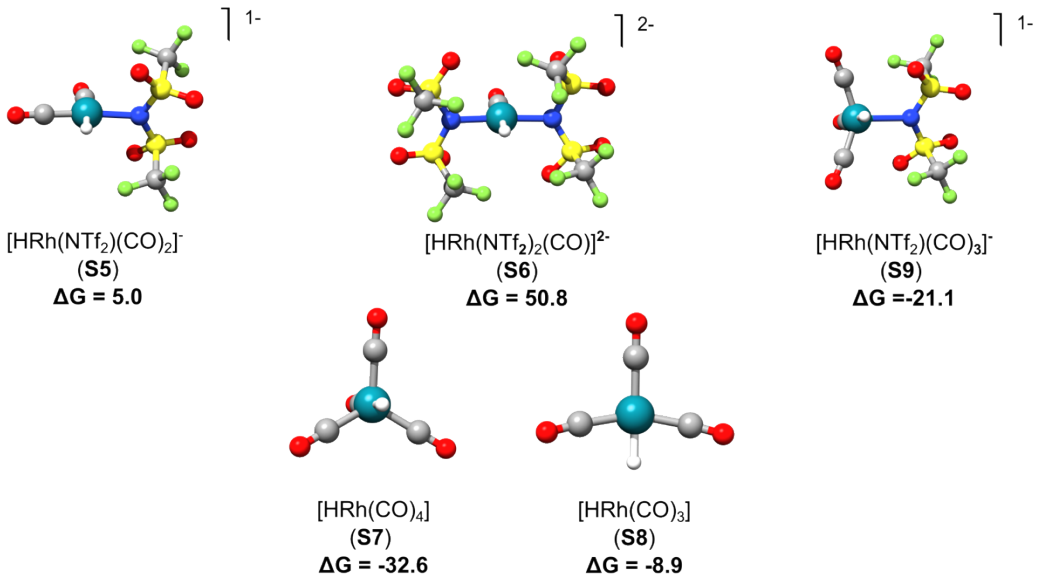

Figure S20: visualisation of all isomers of DFT-optimized species **S5** to **S9.**

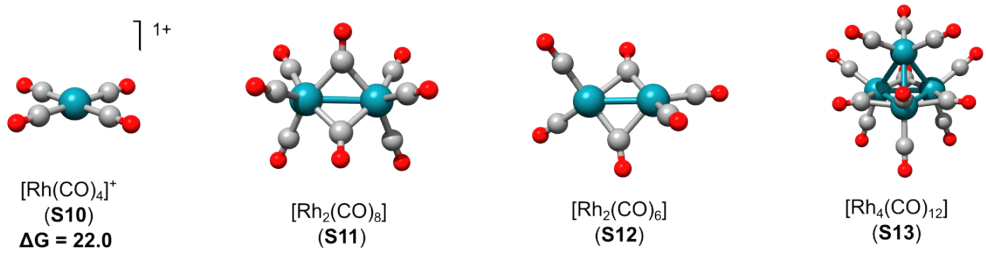

Figure S21: visualisation of all isomers of DFT-optimized species **S10** to **S13.**

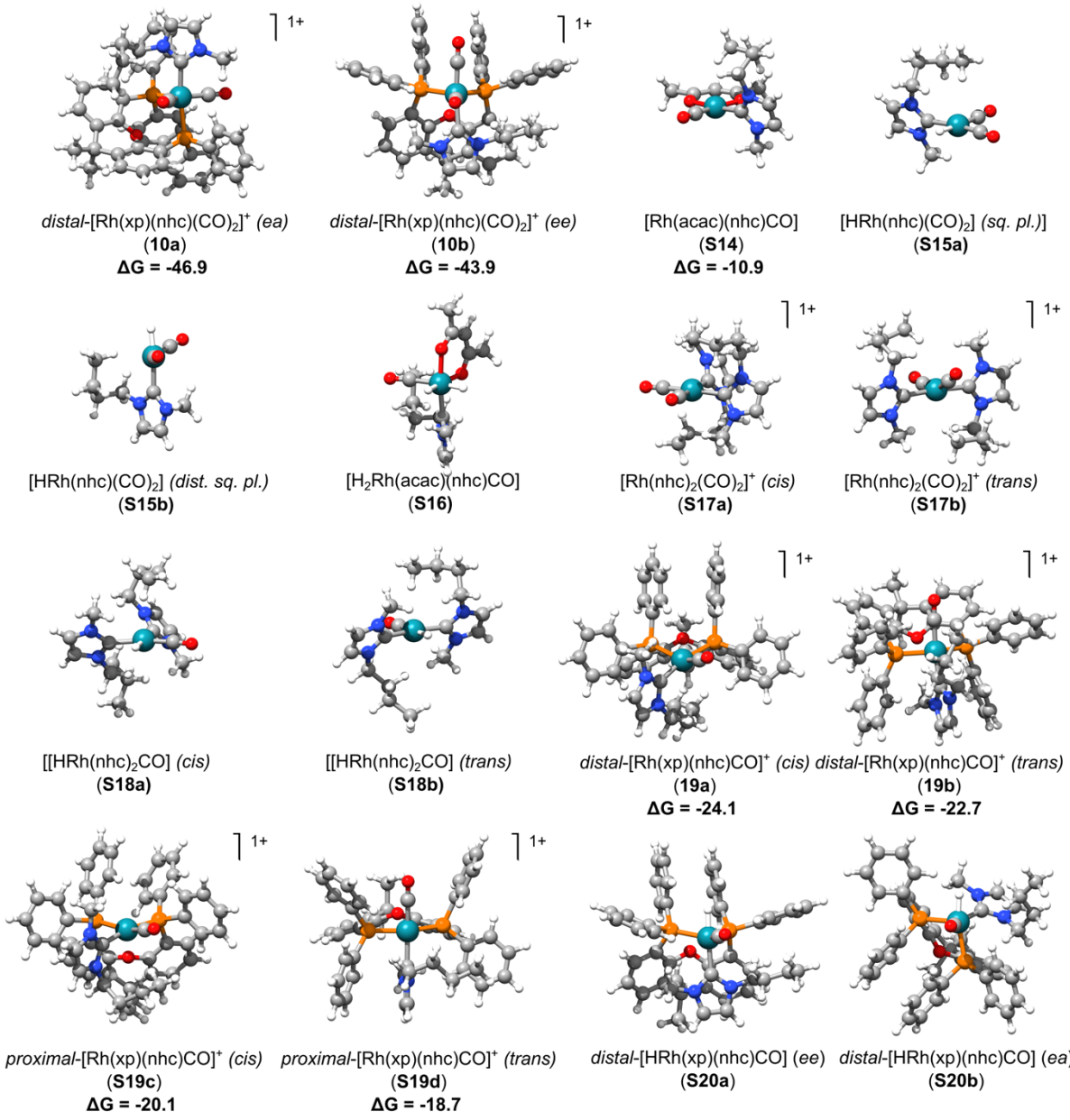

Figure S22: Visualisation of all isomers of DFT-optimized NHC based species**.**

16. Summary of the computed free Energies in solution and the gas-phase for the formation of catalyst precursors (2) and (3)

Table S9: DFT and DLPNO/CCSD(T) computed relative energies for the species involved in the formation of the species **2** and **3**.

	DLPNO-CCSD(T)		ωB97M-V
Species	**ΔG_{gas}**	**ΔG_{solv}**	**ΔG_{solv}**
[Rh(acac)$(CO)_2$]+xp (**1**)	0.00	0.00	0.00
$TS_{(1)-(2)}$	0.94	1.24	1.01
[Rh(acac)$(CO)_2$(xp)] (**2a**)	0.75	-0.38	-1.62
$TS_{(2)-(3)}$	4.26	2.45	1.32
[Rh(acac)(CO)(xp)] (**3b**) + CO	-1.83	-3.84	-4.78
[Rh(acac)(CO)(xp)] (**3a**) + CO	-1.54	-2.04	-3.28
[Rh(acac)(xp)] + 2CO	16.42	17.94	15.24

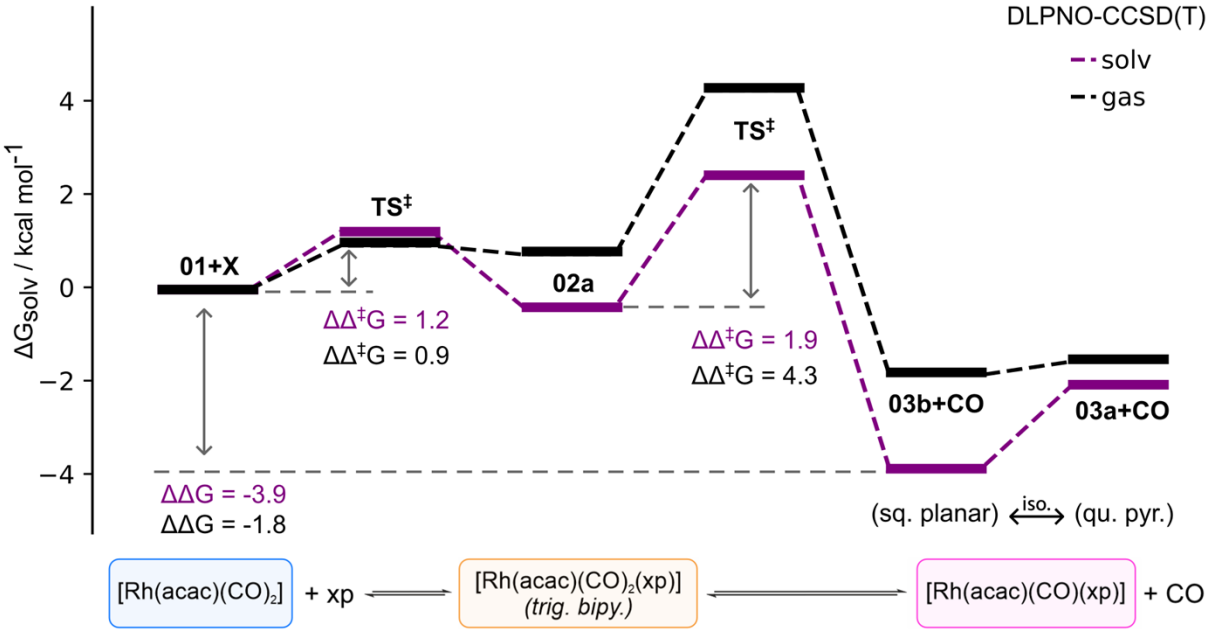

Figure S23: Comparison between gas phase and SMD solvent calculations ($[C_4C_1Im][NTf_2]$ at the DLPNO-CCSD(T)// BP86 level of theory.